Transonic Rudder Buzz on Tailless Flying Wing UAV

Xu Jun (许军)[1], *Ma Xiaoping* (马晓平)[2 *]

1. College of Aeronautics, Northwestern Polytechnical University, Xi′an 710072, P. R. China;
2. UAV Research Institute, Northwestern Polytechnical University, Xi′an 710065, P. R. China

(Received 23 November 2014; revised 21 December 2014; accepted 12 January 2015)

Abstract: Transonic rudder buzz responses based on the computational fluid dynamics or computational structural dynamics (CFD/CSD) loosely method are analyzed for a tailless flying wing unmanned aerial vehicle (UAV). The Reynolds-averaged Navier-Stokes (RANS) equations and finite element methods based on the detailed aerodynamic and structural model are established, in which the aerodynamic dynamic meshes adopt the unstructured dynamic meshes based on the combination of spring-based smoothing and local remeshing methods, and the lower-upper symmetric-Gauss-Seidel (LU-SGS) iteration and Harten-Lax-van Leer-Einfeldt-Wada (HLLEW) space discrete methods based on the shear stress transport (SST) turbulence model are used to calculate the aerodynamic force. The constraints of the rudder motions are fixed at the end of structural model of the flying wing UAV, and the structural geometric nonlinearities are also considered in the flying wing UAV with a high aspect ratio. The interfaces between structural and aerodynamic models are built with an exact match surface where load transferring is performed based on 3D interpolation. The flying wing UAV transonic buzz responses based on the aerodynamic structural coupling method are studied, and the rudder buzz responses and aileron, elevator and flap vibration responses caused by rudder motion are also investigated. The effects of attack, height, rotating angular frequency and Mach number under transonic conditions on the flying wing UAV rudder buzz responses are discussed. The results can be regarded as a reference for the flying wing UAV engineering vibration analysis.

Key words: flying wing unmanned aerial vehicle (UAV); buzz; CFD/CSD; transonic flow; geometric nonlinearities

CLC number: V211.5; O321 **Document code**: A **Article ID**: 1005-1120(2015)01-0061-09

0 Introduction

The new UAV with tailless flying wing has high aspect ratio characteristics, which can lead to more and more serious nonlinear aeroelasticity problems, and it is thus important to accurately calculate the nonlinear aeroelastic responses for the tailless flying wing UAV[1-2].

Lots of aircrafts and missiles had encountered buzz during flight at transonic or low supersonic regions, which could cause crashes[3-4]. Buzz was a forced oscillation[5]. Steger et al.[6-7] studied transonic aileron buzz of the airfoil based on implicit finite-difference computer code. Pak et al.[8] presented the generic National Aero-Space Plane (NASP) configuration control surface buzz, which was based on transonic small disturbance code with an interactive boundary layer and an Euler/ Navier-Stokes (N-S) code. Parker et al.[9-10] studied the effects of NASP wing geometry and aileron hinge stiffness on the buzz behaviors. Nixon[11] proposed a control surface buzz model which was essential for the limit cycle researches. Fuglsang et al.[12] investigated the rudder buzz of T-45A Goshawk aircraft. Oddvar[13] utilized the mixed Eulerian-Lagrangian formulation to study transonic aileron buzz instabilities problems. Su et al.[14] developed a three-dimensional approach to predict transonic flaperon buzz. Liu et al.[15] carried out the hopf-bifurcation analysis to investigate the problems of control surface buzz. Shi et al.[16] addressed the issue of transonic control surface buzz. Zhang et al.[17] numerically analyzed B-type buzz and C-type

* **Corresponding author**: Ma Xiaoping, Professor, E-mail: maxiaoping@nwpu.edu.cn.

How to cite this article: Xu Jun, Ma Xiaoping. Transonic rudder buzz on tailless flying wing UAV[J]. Trans. Nanjing U. Aero. Astro., 2015,32(1):61-69.

http://dx.doi.org/10.16356/j.1005-1120.2015.01.061

buzz. Yang et al.[18] introduced an implicit multiblock aeroelastic solver to the aileron buzz simulations of the supersonic transport model of the national aerospace laboratory of Japan. Tang et al.[19] studied the large aircraft aeroelastic multidisciplinary design optimization.

The literatures about buzz are few, and mostly concentrated on the wing. The buzz responses analysis that considered the detail aircraft structural model had not be published yet. Therefore, this paper mainly discusses the flying wing UAV structural model buzz responsesin detail, as well as the rudder motion constraints at the end of the flying wing UAV rudder structural model. The detailed structural and aerodynamic models are built, and the computational fluid dynamics or computational structural dynamics (CFD/CSD) loosely coupling method is developed for the tailless flying wing UAV buzz analysis. The center finite volume methods are used to solve the Reynolds-averaged Navier-Stokes (RANS) equations. The aerodynamic calculation uses the unstructured dynamic meshes based on the combinations of the spring-based smoothing and local remeshing methods, and also considers the structural geometric nonlinearities in the high aspect ratio flying wing UAV. The interfaces between the structural and aerodynamic domains are built with an exact match surface, where load transferring are performed based on 3D interpolation.

1 CFD/CSD Coupling Method

The aerodynamic structural coupling analysis belongs to the aeroelastic category . There exist two kinds of aerodynamic structural iteration methods. One is the loosely coupling method, and the other the tightly coupling method. It is hard to solve the structural dynamic equations and aerodynamic control equations simultaneously. Hence, the tightly coupling method is not applicable to engineering analysis but only for theoretical investigation. The general method for aircraft aeroelastic calculation is the loosely coupling method, namely solving the structural dynamic equations and aerodynamic control equations independently, and transferring the deformation displacements and aerodynamic forces only on the aerodynamic structural coupling surfaces.

As the aerodynamic structural loosely coupling occurs only on the coupling surfaces, the coupling equations are introduced by equilibrium and compatibility conditions of the interface surfaces. Accordingly the aeroelastic equations and boundary conditions can be represented as

$$\boldsymbol{M}\ddot{\boldsymbol{U}}+\boldsymbol{C}\dot{\boldsymbol{U}}+\boldsymbol{K}\boldsymbol{U}=\boldsymbol{F}(t) \tag{1}$$

$$\frac{\partial}{\partial t}\iiint_{\Omega}\bar{\mathrm{Q}}\,\mathrm{d}\Omega+\iint_{S}(\bar{\mathrm{G}}-\bar{\mathrm{Q}}\,\boldsymbol{q}_b)\cdot\mathrm{d}\boldsymbol{S}=\frac{1}{Re}\iint_{S}\bar{F}^{V}\cdot\mathrm{d}\boldsymbol{S} \tag{2}$$

$$\sigma_s\cdot\boldsymbol{n}=-p\boldsymbol{n},\ \boldsymbol{u}_s=\boldsymbol{u}_F \tag{3}$$

Eq. (1) is the structural dynamic equation, where $\boldsymbol{M}$ is the mass matrix, $\boldsymbol{C}$ the damping matrix, $\boldsymbol{K}$ the stiffness matrix, $\boldsymbol{U}$ the deformation displacement, $\dot{\boldsymbol{U}}$ the deformation velocity, $\ddot{\boldsymbol{U}}$ the deformation acceleration, $\boldsymbol{F}(t)$ the aerodynamic force. Eq. (2) is the integral form of the unsteady N-S equation, where $\bar{G}$ and $\bar{F}^{V}$ are the symmetrical and dissipation terms respectively, Ω the control volume, and $\boldsymbol{S}$ the control surface. Eq. (3) expresses the normal vector equilibrium and displacement compatibility conditions of the interface surface respectively, where σ_s is the interface surfaces structure stresses, $\boldsymbol{n}$ the interface surfaces normal vector, p the interface surfaces aerodynamic pressure, $\boldsymbol{u}_s$ the coupling surfaces structural meshes displacement, and $\boldsymbol{u}_F$ the coupling surface aerodynamic meshes displacement. Based on the CFD/CSD loosely coupling method[19-21], the tailless flying wing UAV rudder responses are studied by solving Eqs. (1—3).

2 Geometry Model of Flying Wing UAV

The wingspan of the tailless flying wing UAV is 15 m, the wing area is 23.5 m^2, and the average aerodynamic chord length is 1 661.1 mm. There are eight boxes and four root ribs in the fuselage. The inside wing structure is composed of wall plates, girders, wing ribs, including four beams and six ribs. The outside wing consists of three beams and sixteen ribs. There are three

rubs behind the outside wing from 2 500 mm to 7 500mm, i. e. rudder, aileron and elevator. The geometry model of the flying wing UAV is shown in Fig. 1.

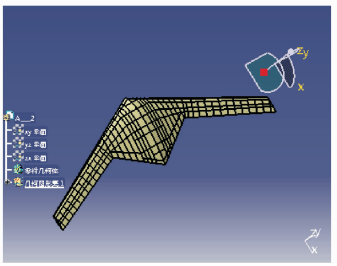

Fig. 1 Geometry model of flying wing UAV

The material of the flying wing UAV is LY2024 with density of 2 770 kg/m^3, elasticity modulus of 71 800 MPa, and Poisson's ratio of 0.33. The model uses a symmetry constraint. The first four modals of the tailless flying wing UAV are 11.645, 22.921, 47.494, and 74.242 Hz, as shown in Fig. 2. The aerodynamic structural coupling surfaces include the fuselage, wing, rudder, aileron, elevator and flap.

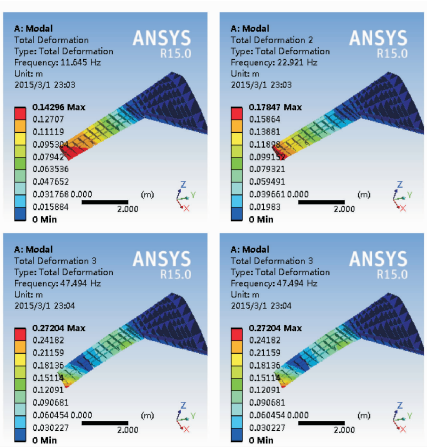

Fig. 2 The first four modals of flying wing UAV

3 Rudder Buzz Response

The constraints of the rudder are illustrated in Fig. 3. The rudder motion conditions are constraint on the flying wing UAV structural model. The rudder deflection motion are constraint on the two end surfaces of the rudder shaft under the cylindrical coordinate, as shown in Fig. 3. The rudder deflection movement is defined in the Y direction in the cylindrical coordinate. Here, the motion equation of the rudder is

$$\beta(t)=\beta_0+\beta_m\sin(\omega t) \tag{4}$$

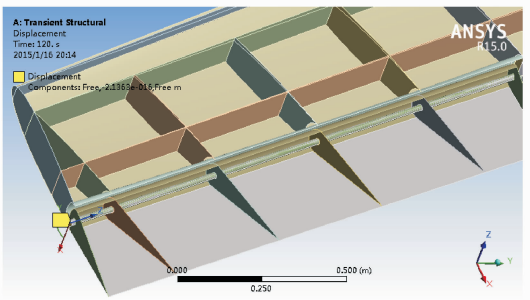

Fig. 3 Constraints of the rudder buzz

where the average rudder angle $\beta_0=0.0°$ and the maximum rudder angle $\beta_m=10.0°$.

The RANS N-S equations with the shear stress transport (SST) aerodynamic turbulence model, and the finite volume method are used to discretize the N-S equation. The second-order lower-upper symmetric-Gauss-Seidel iteration with a Newton-like pseudo time sub-iteration method (LU-SGS-TS) is used. The unstructured dynamic meshes uses the combination of the spring-based smoothing and local remeshing methods.

The CFD/CSD loosely coupling method is developed to calculate the tailless flying wing UAV rudder response. The coupling calculation time step is 0.001 s, and the aerodynamic convergence error is set as 1e−6. The Reynolds-averaged Navier-Stokes RANS equations with the SST turbulence model are used to simulate the aerodynamic. The initial parameters are as follow: $H=8$ km, $Ma_\infty=0.95$, $\omega_n=15$ Hz, $\alpha=0°$, $\xi=0$, $Re=1.612e7$.

The rudder buzz responses are shown in Fig. 4, compared the outside and inside monitoring points of the rudder. The vibration responses

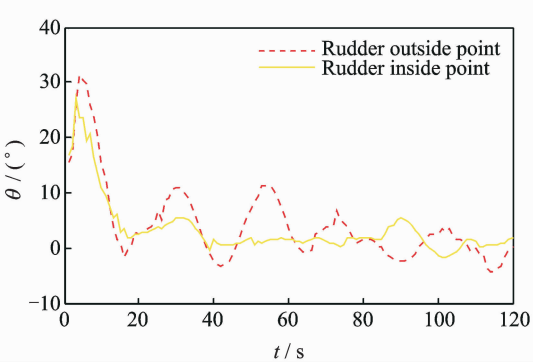

Fig. 4 Rudder buzz responses

of the rudder, aileron, elevator and flap induced by the rudder motion can be found in Fig. 5. Figs. 6, 7 show the surface pressure coefficient and the structural deformation of the flying wing UAV, respectively.

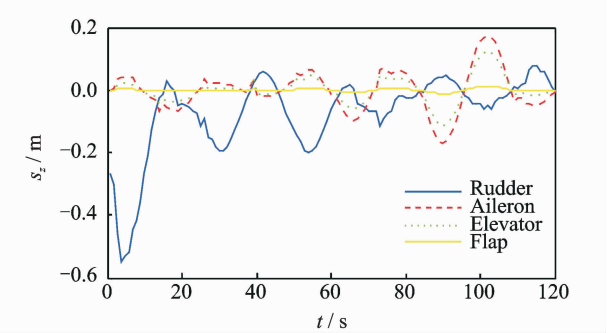

Fig. 5 Vibration responses

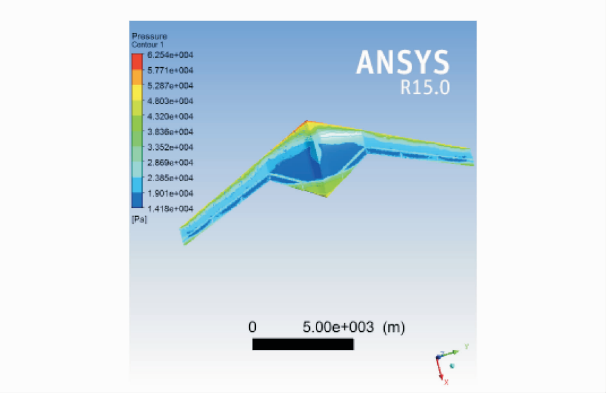

Fig. 6 Surface pressure coefficient of flying wing UAV

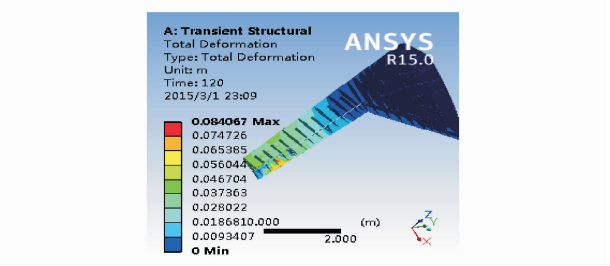

Fig. 7 Structure deformation of flying wing UAV

4 Analyses of Buzz Response Parameters

The effect of attack angle on the rudder bangle time responses is demonstrated in Fig. 8, where both the outside and inside monitoring points of the rudder buzz responses are given. The outside monitoring point of the rudder angle responses is periodic, and different angles have different response amplitudes. As the attack angle increases, the amplitude of rudder angle response decreases.

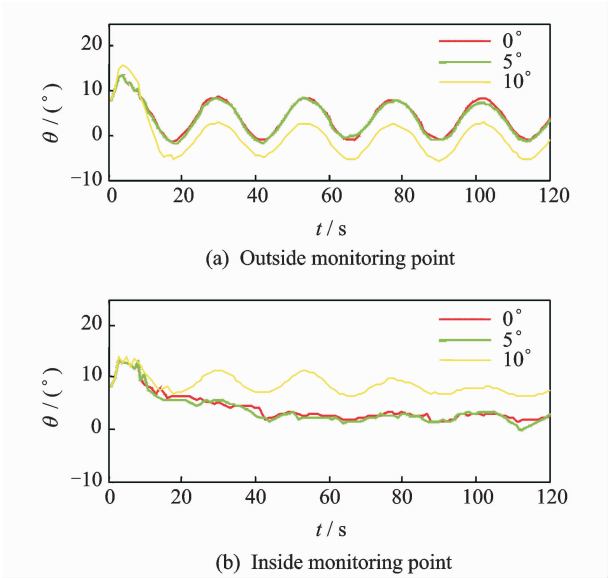

Fig. 8 Effect of attack angle on rudder angle (H = 8 km, Ma_∞ = 0.95, ω_n = 15 Hz, ξ = 0)

The effect of height on the rudder angle time responses is shown in Fig. 9. The outside monitoring point of the rudder angle responses is periodic, and different heights have different response amplitudes. The overall rudder angle response amplitude at 8 km is large, while the overall rudder angle response amplitude at 10 km is small. Fig. 9(b) shows that the rudder angle responses of 10 km and 5 km converge well.

The effect of Mach number on the rudder an-

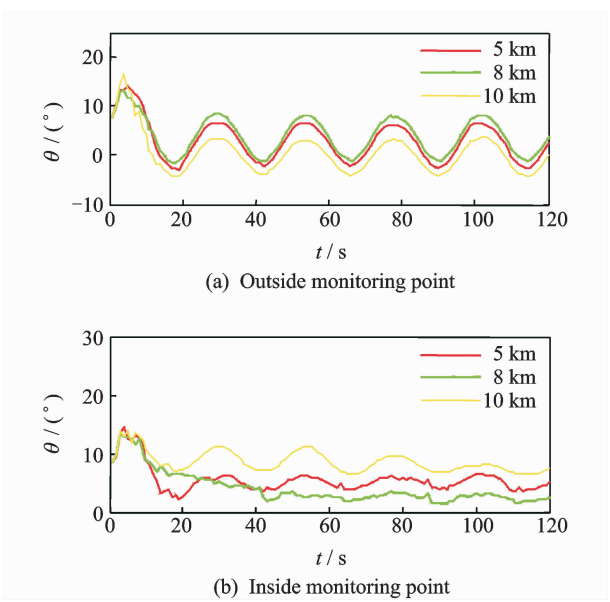

Fig. 9 Effect of height on rudder angle (Ma_∞ = 0.95, ω_n = 15 Hz, α = 0°, ξ = 0)

gle time responses is presented in Fig. 10, where the outside and the inside monitoring points of the rudder buzz responses are provided. In Fig. 10, the outside monitoring point of the rudder angle responses is periodic, and different Mach numbers have different angle response amplitudes. The overall rudder angle response amplitude at $Ma=0.95$ is large, however the amplitude at $Ma=0.85$ is small. Fig. 10(b) shows that the rudder angle responses converge well when $Ma=0.85$ and $Ma=1.05$.

Fig. 11 shows the effect of rotating angular frequency on the rudder angle time responses, where both the outside and the inside monitoring points of the rudder buzz responses are presented. It can be seen that the outer corner of the rudder angle responses is periodic. When the rotating angular frequency differs, the angle response amplitude and the rudder angle response frequency vary correspondingly. Along with the increased rotating angular frequency, the tip angle response frequency ascends gradually, and the peak occurs at the point of 20 rad/s. Fig. 11(b) also shows that the responses of the rudder inside monitoring point converge faster.

Fig. 12 plots the effect of attack on the vibration displacement responses of the rudder, aileron and elevator. Though the rudder vibration displacement responses at different angles show a good periodicity, the responses of aileron and elevator vibration displacement are evidently irregular.

Fig. 13 introduces the effect of height on the vibration displacement responses of the rudder, aileron and elevator. Despite the good periodicity of rudder and aileron vibration displacements at different heights, elevator vibration displacements

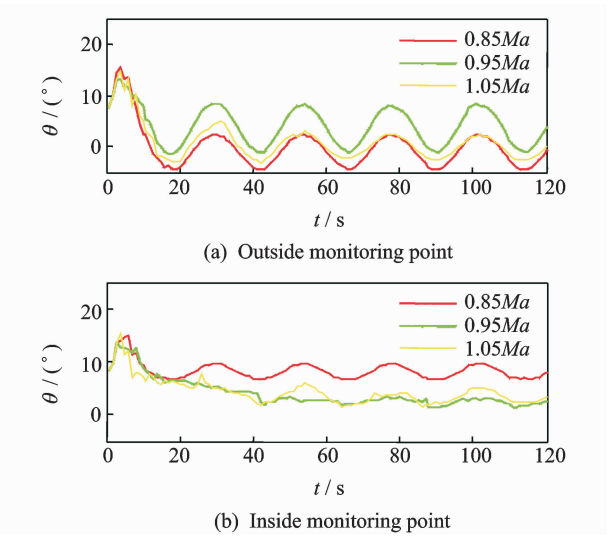

Fig. 10 Effect of Mach number on rudder angle ($H=8$ km, $\omega_n=15$ Hz, $\alpha=0°$, $\xi=0$)

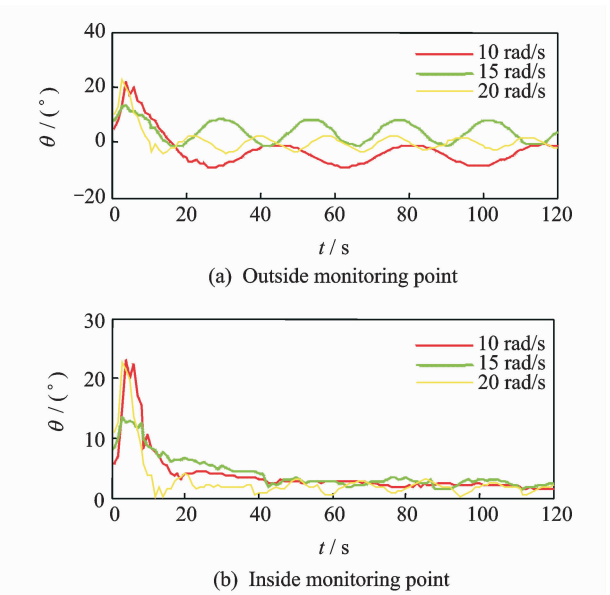

Fig. 11 Effect of rotating angular frequency on rudder angle ($H=8$ km, $Ma_\infty=0.95$, $\alpha=0°$, $\xi=0$)

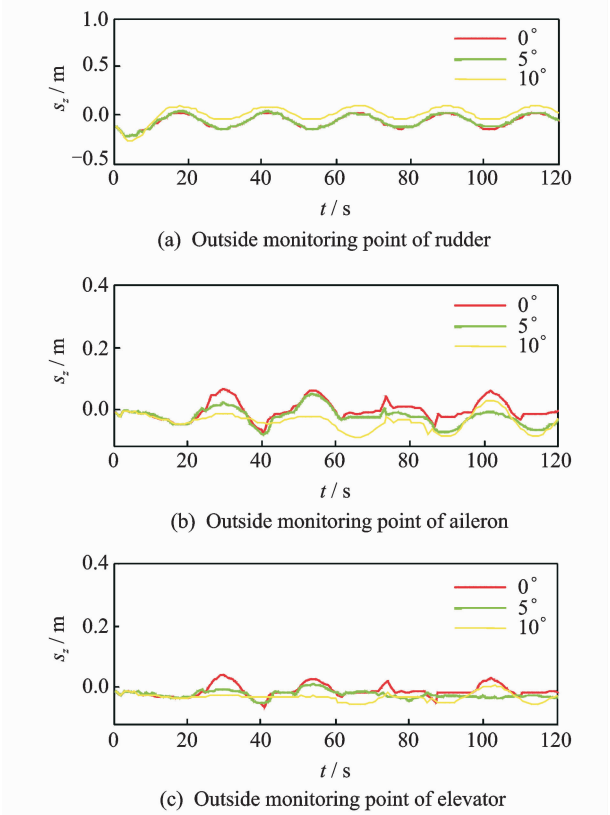

Fig. 12 Effect of attack on vibration displacement ($H=8$ km, $Ma_\infty=0.95$, $\omega_n=15$ Hz, $\xi=0$)

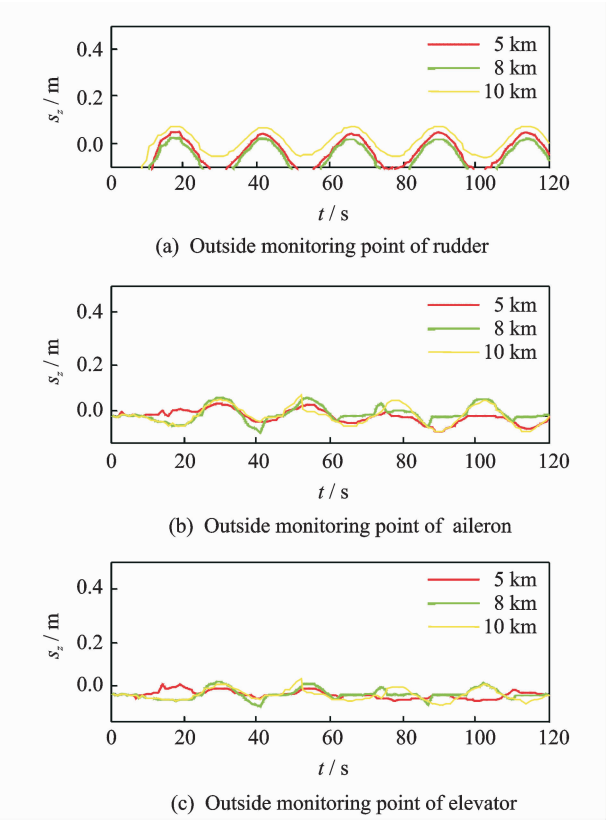

Fig. 13 Effect of height on vibration displacement ($Ma_\infty=0.95$, $\omega_n=15$ Hz, $\alpha=0°$, $\xi=0$)

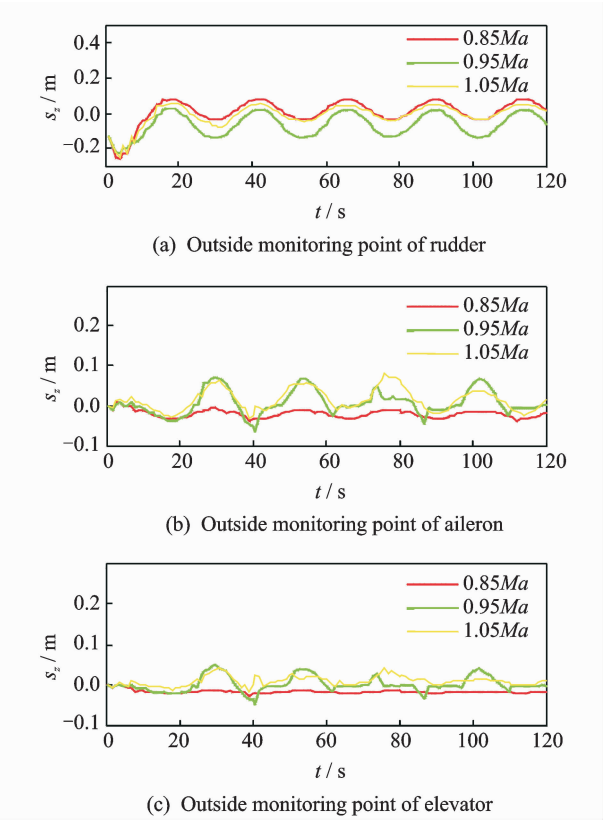

Fig. 14 Effect of Mach number on vibration displacement ($H=8$ km, $\omega_n=15$ Hz, $\alpha=0°$, $\xi=0$)

are irregular.

Fig. 14 shows the effect of Mach number on the vibration displacement responses of the rudder, aileron and elevator. The rudder, aileron and elevator vibration displacements at different heights are periodic, and as the Mach number increases, the vibration displacement responses of the rudder, aileron and elevator responses are obvious.

The effect of rotating angular frequency on the vibration displacement responses of the rudder, aileron and elevator is presented in Fig. 15. The rudder, aileron and elevator vibration displacement response frequencies are different at different rotating angular frequencies. The vibration displacement response frequency rises with the increase of rotating angular frequency.

Figs. 16—19 demonstrate the effects of flight parameters on the rudder angle acceleration of tailless flying wing UAV, i. e. the effect of attack angle on the rudder angle acceleration, the effect

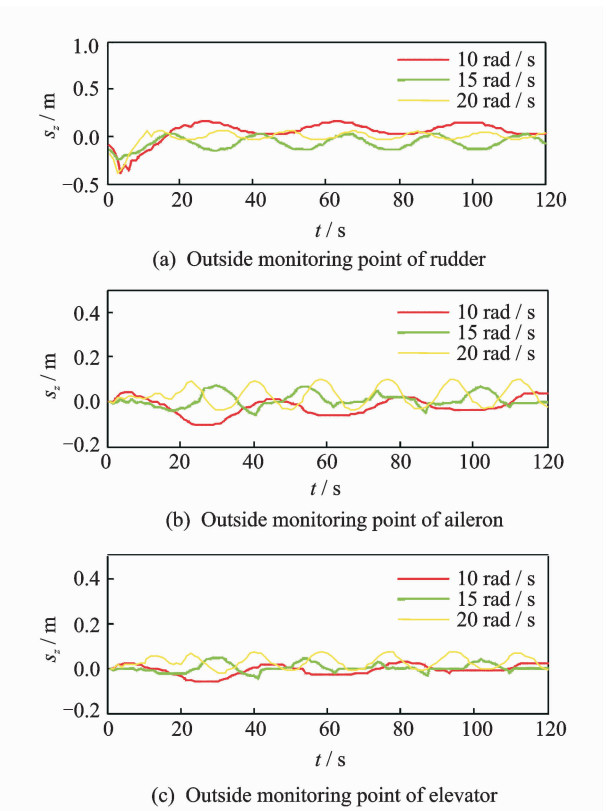

Fig. 15 Effect of rotating angular frequency on vibration displacement ($H=8$ km, $Ma_\infty=0.95$, $\alpha=0°$, $\xi=0$)

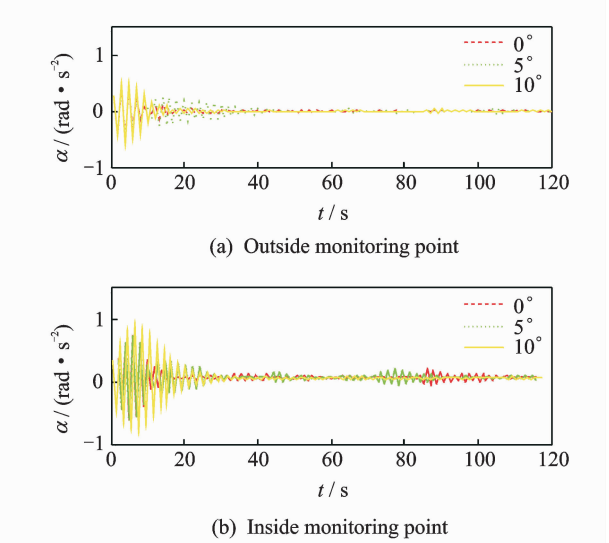

Fig. 16 Effect of attack on rudder angle acceleration (H=8 km, Ma_∞=0.95, ω_n=15 Hz, ξ=0)

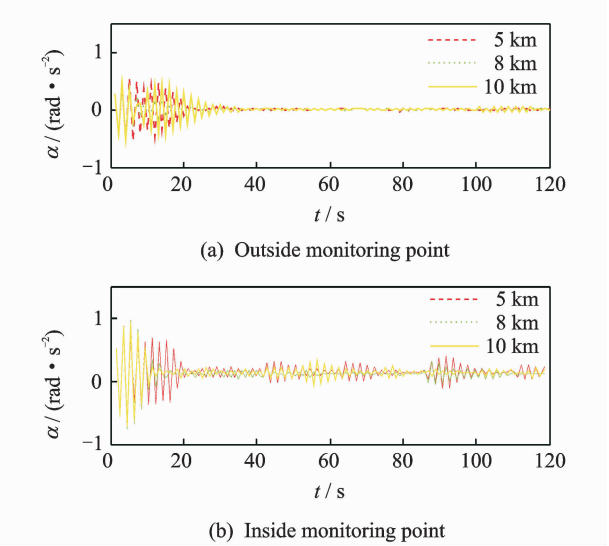

Fig. 17 Effect of height on rudder angle acceleration (Ma_∞=0.95, ω_n=15 Hz, α=0°, ξ=0)

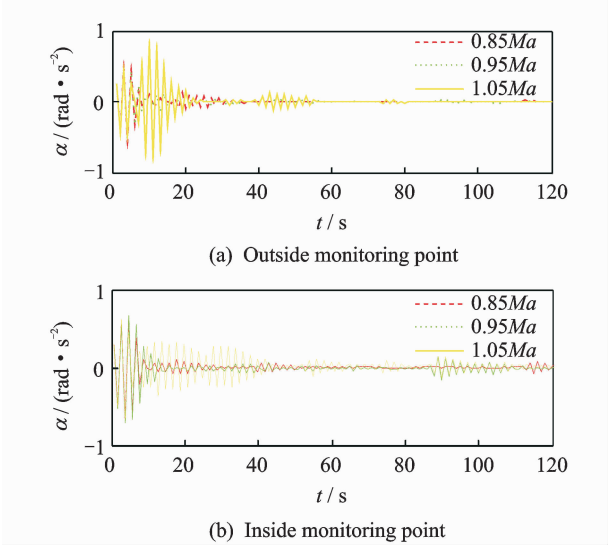

Fig. 18 Effect of Mach number on rudder angle acceleration (H=8 km, ω_n=15 Hz, α=0°, ξ=0)

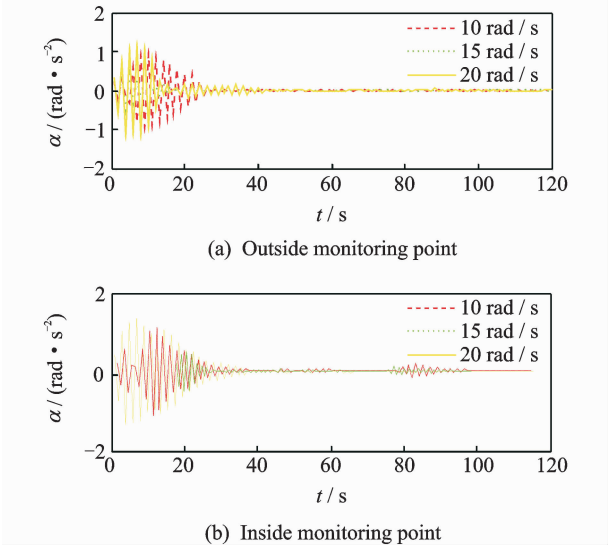

Fig. 19 Effect of rotating angular frequency on rudder angle acceleration (H=8 km, Ma_∞=0.95, α=0°, ξ=0)

of height on the rudder angle acceleration, the effect of Mach number on the rudder angle acceleration, and the effect of rotating angular frequency on the rudder angle acceleration, respectively.

Moreover, Figs. 20—23 show the effect of parameters on the vibration acceleration of tailless flying wing UAV , namely, the effect of attack angle, the effect of height, the effect of Mach number, and the effect of rotating angular frequency on the vibration acceleration, respectively.

5 Conclusions

(1) The detailed structure and aerodynamic model are developed to study the rudder buzz responses of the UAV with tailless flying wing by using the CFD/CSD coupled method.

(2) The effect of rotation angular frequency has the greatest influence on the buzz response frequency than other parameters. As the rotation angle frequency goes up, both the buzz angle response and displacement response frequency increase correspondingly. However, the height,

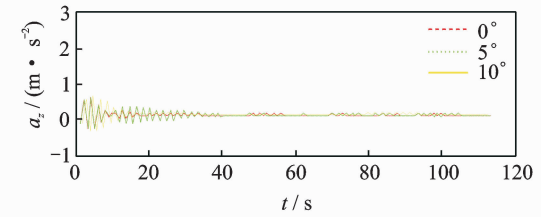

(a) Outside monitoring point of rudder

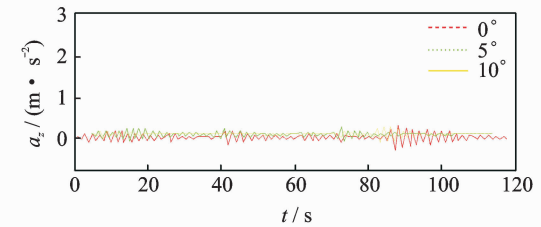

(b) Outside monitoring point of aileron

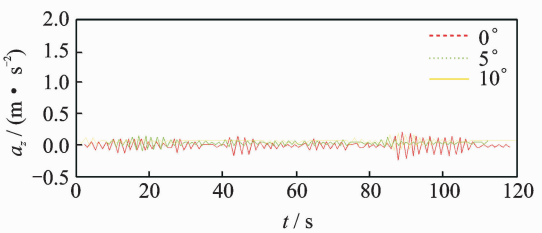

(c) Outside monitoring point of elevator

Fig. 20 Effect of attack on vibration acceleration (H=8 km, Ma_∞=0.95, ω_n=15 Hz, ξ=0)

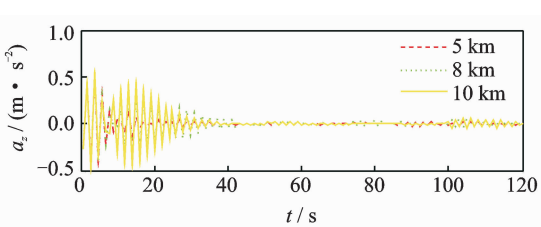

(a) Outside monitoring point of rudder

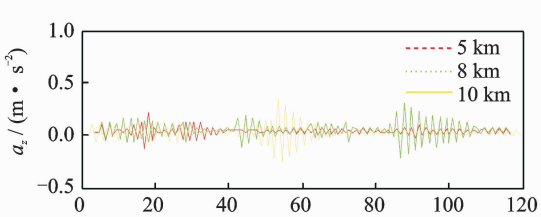

(b) Outside monitoring point of aileron

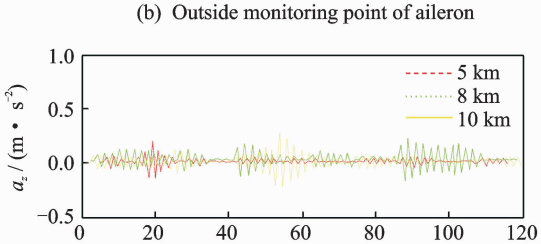

(c) Outside monitoring point of elevator

Fig. 21 Effect of height on vibration acceleration (Ma_∞=0.95, ω_n=15 Hz, α=0°, ξ=0)

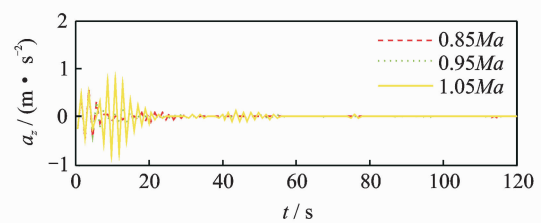

(a) Outside monitoring point of rudder

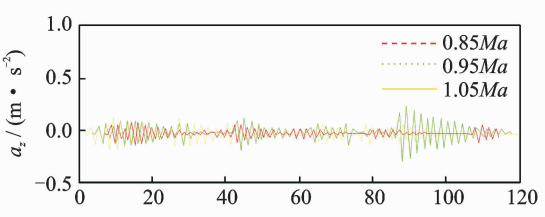

(b) Outside monitoring point of aileron

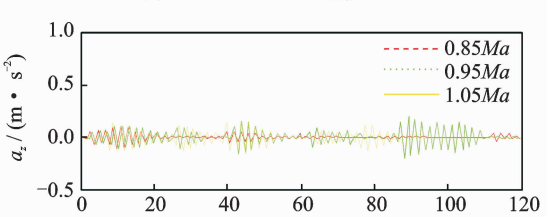

(c) Outside monitoring point of elevator

Fig. 22 Effect of Mach number on vibration acceleration (H=8 km, ω_n=15 Hz, α=0°, ξ=0)

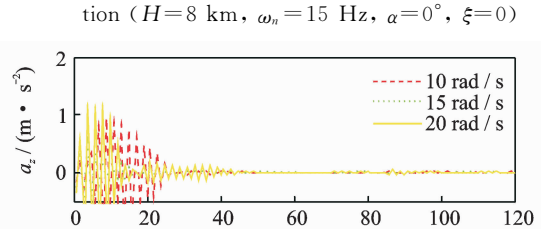

(a) Outside monitoring point of rudder

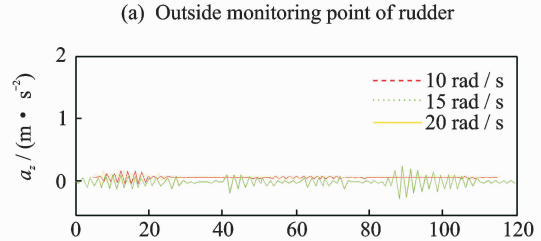

(b) Outside monitoring point of aileron

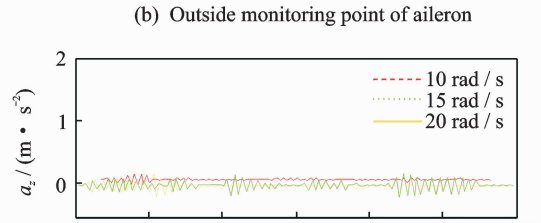

(c) Outside monitoring point of elevator

Fig. 23 Effect of rotating angular frequency on vibration acceleration (H=8 km, Ma_∞=0.95, α=0°, ξ=0)

Mach number and attack angle do not affect the frequency of the buzz angle response and displacement response.

(3) Although providing a reasonable reference for the flight test data, this paper only detailedly discusses the buzz responses induced by the rudder rotation, without referring to the buzz responses induced by elevator, aileron and flap, which should be one of the research directions for further investigation in this field.

Acknowledgements

This work was supported by the Natural Science Foundation of China (No. 61074155) and the Shaanxi Provincial Natural Science Foundation of China (No. 2013JM015).

References:

[1] Dowell E, Edwards J, Strganac T. Nonlinear aeroelasticicy[J]. Journal of Aircraft, 2003,40(5): 857-874.

[2] Dowell E. A modern course in aeroelasticity[M]. Third Edition. [S. l.]:Kluwer Academic Publishing Inc, 1995:215-263.

[3] Sun Yongjun, Wang Dongsen. Analysis study on transonic speed equal amplitude vibration of a certain type of aircraft[J]. Chinese Journal of Applied Mechanics, 2001, 18:203-206. (in Chinese)

[4] North Atlantic Treaty Organization. The effects of buffeting and other transonic phenomena on maneuvering combat aircraft[M]. Li Ming, Hu Bingke, Chen Ruixi, Translated. Beijing: International Aviation Newsroom, 1980: 204-206. (in Chinese)

[5] Lambourne N C. Control-surface buzz[R]. R&M No. 3364, 1964.

[6] Steger J L, Bailey H E. Calculation of transonic aileron buzz[R]. AIAA-79-0134, 1979.

[7] Steger J L, Bailey H E. Calculation of transonic aileron buzz[J]. AIAA Journal, 1980, 18(3): 249-255.

[8] Pak Chen-gi, Baker M L. Control surface buzz analysis of a generic NASP wing[R]. AIAA Paper 2001-1581, 2001.

[9] Parker E C, Spain C V, Soistmann D L. Experimental transonic buzz characteristics of a clipped delta-wing model with a full-span aileron[R]. NASP CR-1083, 1990.

[10] Parker E C, Spain C V, Soistmann D L. Aileron buzz investigated on several generic NASP wing configurations[R]. AIAA-91-0936-CR, 1991.

[11] Nixon D. An analytic model for control surface buzz [R]. AIAA98-0417,1998.

[12] Fuglsang D F, Brase L O, Agraswal S. A numerical study of control surface buzz using computational fluid dynamic methods[R]. AIAA-92-2654, 1992.

[13] Bendiksen O O. Nonclassical aileron buzz in transonic flow[R]. AIAA-93-1479, 1993.

[14] Su Shen-Jwu, Chen P C. Equivalent strip method of transonic flaperon buzz[R]. AIAA-96-0166, 1996.

[15] Liu Qiangang, Dai Jie, Bai Junqiang. Hopf-bifurcation analysis of transonic control surface buzz and investigation of the influence of structural parameters on buzz characteristics[J]. Acta Aeronautica et Astronautica Sinica, 1999, 20(6): 527-532. (in Chinese)

[16] Shi Aiming, Yang Yongnian, Ye Zhengyin. Investigated of control surface buzz in transonic flow[J]. Journal of Northwestern Polytechnical University, 2004, 22(4): 525-528. (in Chinese)

[17] Zhang Weiwei, Ye Zhengyin, Shi Aiming, et al. Numerical analysis for B-type buzz and C-type buzz based on Euler codes[J]. Journal of Vibration Engineering, 2005, 18(4): 458-464. (in Chinese)

[18] Yang Guowei, Obayashi Shigeru. Aileron buzz simulation using an implicit multiblock aeroelastic solver [J]. Journal of Aircraft, 2003, 40(3): 580-589.

[19] Tang Changhong, Wan Zhiqiang. Application of hybrid genetic algorithm in aeroelastic multidisciplinary design optimization of large aircraft[J]. Transactions of Nanjing University of Aeronautics & Astronautics, 2013, 30(2): 109-118.

[20] Meng Lingbing, Ang Haisong, Xiao Tianhang. Numerical simulation of fluid-structure interaction for flexible wing UAV[J]. Journal of Nanjing University of Aeronautics & Astronautics, 2013, 45(5): 621-627. (in Chinese)

[21] Chen Meng, Wang Lu, Cheng Han, Yu Li. Numerical prediction analysis of parachute inflation process using fluid-structure interaction method[J]. Journal of Nanjing University of Aeronautics & Astronautics, 2013, 45(4): 515-520. (in Chinese)

(Executive editor: Zhang Tong)